Nuclear Instruments and Methods in Physics Research A 785 (2015) 191–196

Contents lists available at ScienceDirect

Nuclear Instruments and Methods in Physics Research A

journal homepage: www.elsevier.com/locate/nima

Increased photoelectron transmission in High-pressure photoelectron spectrometers using "swift acceleration"

Mårten O.M. Edwards [a], Patrik G. Karlsson [a], Susanna K. Eriksson [b], Maria Hahlin [c], Hans Siegbahn [c], Håkan Rensmo [c], Juhan M. Kahk [d], Ignacio J. Villar-Garcia [d], David J. Payne [d], John Åhlund [a,*]

[a] VG Scienta AB, Box 15120, 750 15 Uppsala, Sweden
[b] Department of Chemistry-Ångström, Uppsala University, Box 523, 751 20 Uppsala, Sweden
[c] Department of Physics and Astronomy, Uppsala University, Box 516, 751 20 Uppsala, Sweden
[d] Department of Materials, Imperial College London, Exhibition Road, London SW7 2AZ, UK

ARTICLE INFO

Article history:
Received 16 February 2015
Accepted 22 February 2015
Available online 2 March 2015

Keywords:
High-pressure X-ray photoelectron spectroscopy
Photoelectron spectroscopy
Scientific instrumentation
Spectrometer
Charge particle analyser

ABSTRACT

A new operation mode of a HPXPS (high-pressure X-ray photoelectron spectroscopy) analyzer is evaluated on a HPXPS system fitted with an Al Kα X-ray source. A variety of metal foil samples (gold, silver and copper) were measured in different sample gas environments (N_2 and H_2O), and a front aperture diameter of 0.8 mm. The new design concept is based upon "swiftly" accelerating the photoelectrons to kinetic energies of several keV after they pass the analyzer front aperture. Compared to the standard mode, in which the front section between the two first apertures is field-free, this gives a wider angular collection and a lower tendency for electron losses in collisions with gas molecules within the analyzer. With the swift-acceleration mode we attain, depending on the experimental conditions, up to about 3 times higher peak intensities in vacuum and about 10 to 20 times higher peak intensities in the 6–9 mbar regime, depending on kinetic energy. These experimental findings agree well with simulated transmission functions for the analyzer. The new mode of operation enables faster data acquisition than the standard mode of operation, particularly valuable in a home laboratory environment. Further demonstrations of performance are highlighted by measurements of the valence band structure in dye-sensitized solar cell photoelectrodes under a 2 mbar H_2O atmosphere, a molecularly modified surface of interest in photoelectrochemical devices.

1. Introduction

High pressure X-ray photoelectron spectroscopy (HPXPS) has in recent years become a powerful and increasingly popular method for studying chemical species at solid and liquid surfaces at pressures closer to ambient conditions. This has created an opportunity to study a wide range of materials and phenomena, related to surface gas and liquid interactions, that previously have not been possible to study with conventional ultra high vacuum (UHV) photoelectron spectroscopy [1].

Photoelectrons with kinetic energies up to a few keV are more strongly scattered by gas molecules due to higher electron scattering cross-sections at these energies. This result in photoelectron signal intensities, many orders of magnitude lower than in standard XPS measurements. This is a reason why most HPXPS experiments are performed at synchrotron facilities with high photon fluxes by teams specializing in large-scale UHV instrumentation [1–6]. To become a widespread laboratory-based method, available to the wider scientific and industrial communities, it is crucial that high-pressure spectra can be recorded on a reasonable timescale [2,7,8] In this work we present an analyzer high-voltage operation mode "swift acceleration" that widens the angular collection and drastically reduces the internal electron collision losses found in lab-based HPXPS analyzers, and consequently greatly reduces the data acquisition times. The swift acceleration mode differs from the standard mode of operation in that it has a high voltage potential close to the first aperture of the instrument. This allows for faster acceleration of the electrons in this mode and hence a higher transmission is realized. In this work we compare the new swift acceleration lens table with the standard transmission mode lens table, used in Ref. [6], with regard to the analyzer transmission and spectral quality for a wide range of analyzer slit-widths, pass energies, and sample pressures. The swift mode of operation was evaluated using gold, silver and copper samples under various nitrogen and water pressures and the swift acceleration mode performance was further validated

* Corresponding author.
E-mail address: john.ahlund@vgscienta.com (J. Åhlund).

http://dx.doi.org/10.1016/j.nima.2015.02.047
0168-9002/

using a photoelectrochemically active interface consisting of a mesoscopic TiO_2 photoelectrode sensitized with a Ru-based dye molecule under a water vapor pressure of 2 mbar. Such electrochemical systems are interesting for energy applications such as molecular solar cells and are also closely related to many systems used for photocatalysis.

We find that with the swift-acceleration mode we attain, depending on the experimental conditions, up to about 3 times higher peak intensities in vacuum and in the range of 10 to almost 20 times higher peak intensities in the 6–9 mbar regime. No Corona/dielectric breakdown was observed during any of the experiments, due to the high potential in the front of the instrument. This enables stable operation with higher transmission using the swift acceleration mode. A consequence of the extended pressure regime is that larger front cone apertures can be used in HPXPS, giving improved electron collection and facilitating the use of large X-ray sample spots.

2. Experimental

The experiments were performed at the HPXPS system at VG Scienta AB in Uppsala, Sweden, whose main components are a Scienta MX 650 HP X-ray source, a Scienta R4000 HiPP-2 electron analyzer, an analysis chamber with a manipulator-controlled sample holder array, and a preparation chamber for sample loading. For a detailed description and schematic views of the set-up, see Ref. [6]. The peak energy and width of the Bragg reflected Al Kα radiation from the X-ray monochromator is 1486.7 eV and ~200 meV, respectively, and the incidence angle on the sample is 62.5° for central X-rays. The X-ray source settings (200 W power, 12.0 kV electron acceleration voltage) and the alignment of the whole source and the monochromator crystals were kept constant throughout the experimental series.

The electron analyzer consists of (i) a straight energy-retarding and differentially pumped section and (ii) an energy-analyzing 180° hemisphere with a mean radius of 200 mm, nine interchangeable slits, and a 2D MCP/CCD type detector. Emitted photoelectrons from the sample enter the differential pumping stage lens through a small aperture in the conical front. For operation in different sample pressure regimes several exchangeable analyzer front cones with different aperture diameters are available [6]. The analyzer slit width can be varied from 200 μm to 4 mm. For these experiments a set of curved slits (0.1 mm, 0.2 mm, 0.3 mm, 0.4 mm and 0.8 mm) and a set of straight slits (1.5 mm, 2.5 mm and 4 mm) were used. The analyzer can be operated using pass energies from 50 to 500 eV [6]. The so-called lens table describes the optimum high-voltage configuration of the analyzer lens elements, and its dependence on kinetic energy and pass energy. The lens table is a unique property for a specific analyzer type which is derived through electron-optics simulations of element voltages for a limited number of kinetic energies and interpolation between the simulated points [9,10]. Of particular interest in this work are the geometry and the voltage configuration of the elements at the front of the analyzer. Another conical element, with a several mm wide central circular opening, is situated 10 mm downstream from the front cone, and on further downstream there is also a mesh lens element, electrically connected to the second cone. The front cone is permanently grounded, and in previous work [6] the second cone and the mesh element were also grounded to keep the zone from the sample to the mesh field-free. This keeps aberrations at a minimum and is, in particular, advantageous for angular measurements. Associated with this field-free front operation are standard-operation lens tables, e.g. transmission mode and angular mode lens tables. To attain higher analyzer transmission we have developed a swift-acceleration operation mode, wherein the electrons are accelerated from ground to around 4.5 keV, about three times higher than the Al Kα X-ray excitation energy, along a 10 mm path between the front (first) and second cone. The lens table associated with this mode of operation is tailored for Al Kα X-ray excitation sources to further streamline the use of home laboratory and soft X-ray HPXPS systems.

The modes of operation were evaluated using silver, gold, and copper foil samples (99.95% from A. Rasmussen a.s.; 99.99% from KarAna AB; and 99.99% from Goodfellow Ltd., respectively). Nitrogen (99.999% Alphagaz 1™ from Air Liquide AB) was used as the sample gas in the analysis chamber unless explicitly stated otherwise. Complementary tests are performed with water vapor as the sample gas. Water vapor from heated water in a test tube is introduced in the analysis chamber through a leak valve. Prior to the measurements dissolved gases in the test tube water are eliminated by repeated freeze-pump-thaw cycles. To keep sample contamination at a minimum the metal sample surfaces are mechanically etched prior to insertion into vacuum. In the experiments the sample surface is always oriented normal to the axis of the straight retarding analyzer section. The dye-sensitized solar cell sample consisting of a mesoscopic TiO_2 photoelectrode sensitized with a Ru-based dye molecule was prepared in a similar way as described in [11,12]. The sample was measured in vacuum and in a 2 mbar H_2O atmosphere.

A 0.8 mm diameter front cone is used throughout the measurement series and, if not explicitly stated otherwise, the sample surface is located at a distance of one front cone diameter from the front cone (i.e. 0.8 mm). At this distance the sample surface is in the entrance focal point of the analyzer, and furthermore the true pressure at the sample surface is approximately equal (less than 10% difference) to the measured pressure in the rest of the analysis chamber [13]. For all metal samples, spectra were acquired with an energy step size of 0.05 eV (0.54 eV for pass energy 300 eV) and a dwell time of 1 s. The Ag, Au, and Cu regions were recorded with windows of 13 eV, 10 eV, and 13 eV, respectively. The full width half maximum (FWHM) and the peak intensities, expressed as the area under the peak, are evaluated by fitting the spectral line with a Voigt function using a Shirley background.

At no time during the experiments, discharges or arcing was observed despite the fact that these types of problems are quite common in the field of HPXPS. Discharges are more likely to occur in HPXPS than XPS due to the higher pressures in the former, and the risk is especially high in the Corona discharge region. Discharges will show up as spikes in the recorded data and they might cause malfunction or even destruction of the equipment since induced currents stress the high voltage electronics of the analyzer. In the present system, red LED's on the high voltage cards is able to indicated discharges or other instabilities, but no such conditions have been observed.

3. Results and discussion

3.1. Effects on line shape for the different lens modes

Fig. 1 displays a set of normalized Ag 3d spectra for the standard mode of operation and the swift acceleration mode for a set of different slits using a pass energy of 200 eV. For small slit sizes, e.g. 0.3 mm (Fig. 1a) to fairly large slit sizes of i.e. 1.5 mm (Fig. 1b) the swift acceleration mode and standard mode peak line profiles are almost identical. For larger slits the peak profiles shows an asymmetry, with a tail on the low-kinetic-energy side (high binding energy side), as seen in Fig. 1c where the largest slit (4.0 mm) of the analyzer is used. It is also worth noting that the spectral line shape and position of the asymmetric Ag $3d_{5/2}$ peak (recorded using the 4.0 mm slit) does not change with sample distance. That is, up to slit widths of 1.5 mm (the smallest straight slit) the swift-acceleration lens table can be used without precautions regarding the asymmetry, which is further supported by measurements using pass

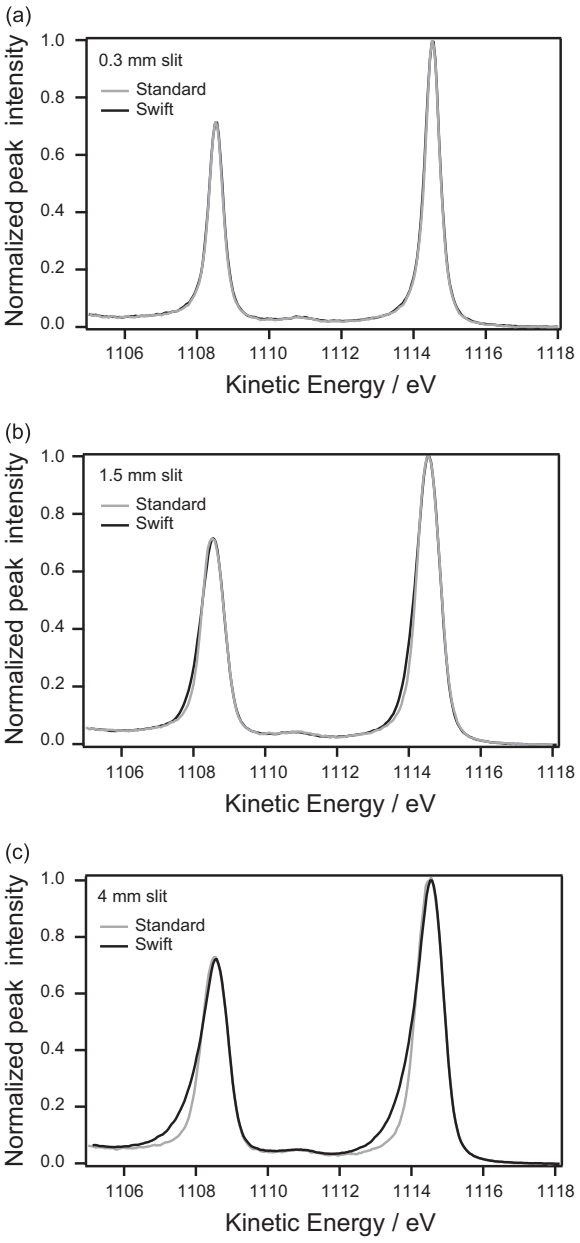

Fig. 1. Ag 3d peak profiles obtained with the standard and swift-acceleration lens tables in vacuum. The spectra were recorded at a pass energy of 200 eV using 0.3 (a), 1.5 (b), and 4.0 mm slits (c).

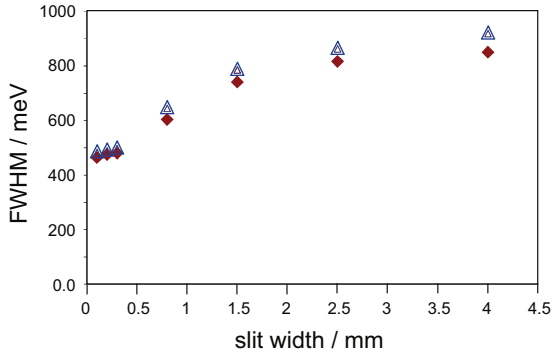

Fig. 2. Measured Ag $3d_{5/2}$ resolution as a function of slit width. The measurements were done in vacuum using a pass energy of 200 eV. Data from the standard lens table and the swift-acceleration table are represented by red filled diamonds and blue open triangles, respectively. (For interpretation of the references to color in this figure legend, the reader is referred to the web version of this article.)

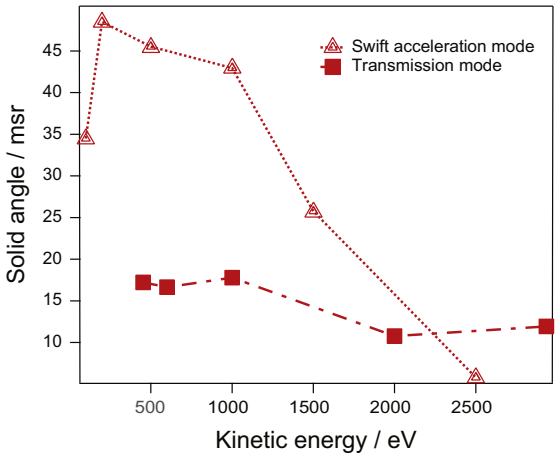

Fig. 3. Simulated mean solid angle collection efficiency as a function of photoelectron kinetic energy for a 0.8 mm front cone, 200 eV pass energy and a 1.5 mm slit. Data from the standard and the swift-acceleration lens tables are represented by filled squares and open triangles, respectively.

energies of 50 eV–500 eV (not shown here) and kinetic energies (550 eV for Cu $2p_{3/2}$ and 1399 eV for Au $4f_{7/2}$). In general there is little or no meaning of using larger slits than 1.5 mm with the Scienta R4000 HiPP-2 electron analyzer, irrespective of which lens table is used, as this only has a minor effect on the peak resolution and intensities, which can be concluded from Fig. 2 and Fig. 4 and also is discussed in more detail in Ref. [6].

A detailed account of the peak resolution dependence on pass energy and slit widths in the standard operation mode is given in [6]. In Fig. 2 the FWHM data of fitted Voight profiles for Ag $3d_{5/2}$ using 200 eV pass energy measurements in vacuum (without a sample gas) is displayed versus slit width for the standard and swift-acceleration modes of operation. There is a change in the peak width behavior around 0.8 mm slit width. Equal peak widths in the swift-acceleration and standard modes are found below this breakpoint, whilst somewhat wider swift-acceleration peaks are found above. However, the broadening is less than 50 meV and will most likely be insignificant during most measurement situations. These results clearly demonstrate that the swift-acceleration mode has little or no additional effects on the line shape of acquired spectra with respect to the standard lens table of the instrument for slits ≤ 1.5 mm.

3.2. Intensities for the different lens modes: in vacuum

Results from electron-optic simulations using a home-made software package [14] are given in Fig. 3. The collection efficiency of the two investigated lens tables in vacuum is displayed as the mean solid angle versus electron kinetic energy. It is seen that the swift-acceleration table is about 2–3 times more efficient compared to the standard table in the regime that is observable when using an Al Kα X-ray excitation source. The acceptance angle of the standard/transmission mode of operation is 26° whereas the acceptance angle for the swift acceleration mode is 40°. The simulations are performed under similar conditions as the present experiments using a 0.8 mm front cone aperture, a 1.5 mm analyzer slit, and 200 eV pass energy. The spot size for the calculation was chosen to match the spot of the front cone as the electrons emitted outside the first cone is estimated not to enter the lens [2]. The transmission function is presented as the mean solid angle as a function of kinetic energy [14].

A detailed account of peak intensity relations in the standard operation mode is given in [6]. The transmission enhancement with the swift-acceleration mode, as compared to the standard operation

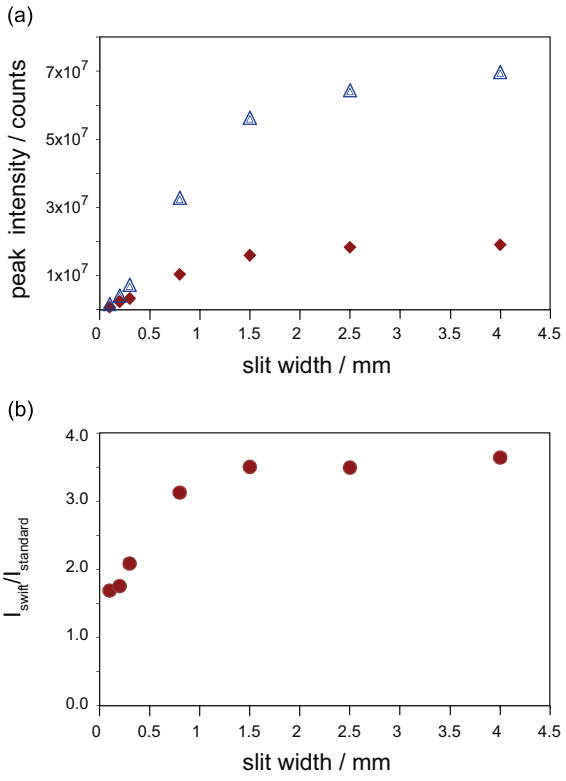

Fig. 4. Peak intensity (a) and peak intensity enhancement (b) as a function of slit width for the Ag $3d_{5/2}$ peak in vacuum measurements using a pass energy of 200 eV. Data from the standard lens table and the swift-acceleration table are represented by filled diamonds and open triangles, respectively. The intensity enhancement of the swift acceleration mode compared to the standard table ($I_{swift}/I_{standard}$) in figure b are illustrated by filled circles.

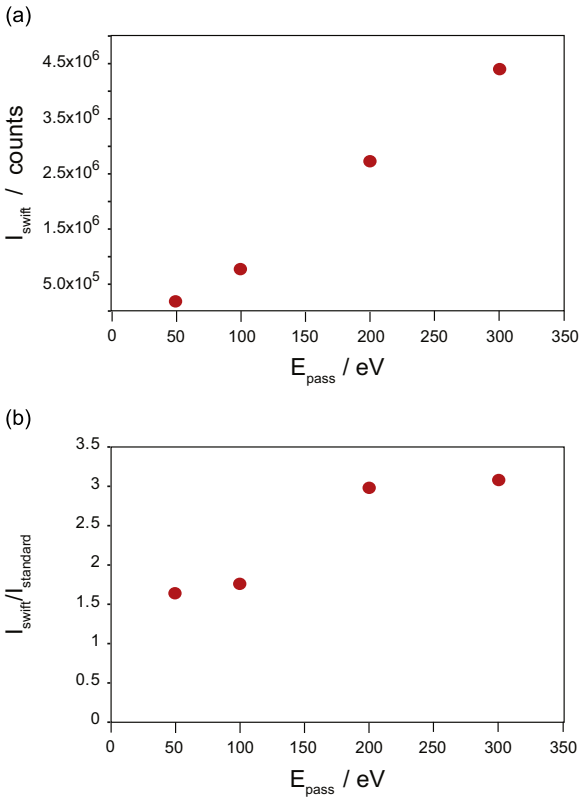

Fig. 5. Swift-acceleration peak intensity (a) and peak intensity enhancement compared to standard mode of operation (b), as a function of pass energy for the Ag $3d_{5/2}$ peak in vacuum measurements using a slit width of 1.5 mm.

mode, may be described by intensity ratios $I_{swift}/I_{standard}$ between photoelectron peaks recorded under the same experimental conditions (Fig. 4). In Fig. 4a the Ag $3d_{5/2}$ peak intensities from the different modes are displayed for 200 eV pass energy measurements in vacuum (without a sample gas) versus slit width along with individual peak intensities, while Fig. 4b displays the enhancement ($I_{swift}/I_{standard}$) of the swift acceleration mode in comparison to the standard mode. It is seen that the wider angular collection in the swift-acceleration mode has a striking effect in the whole range, and the enhancement grows with slit width and reaches a plateau at slightly above 3 for a slit width of 1.5 mm, which is in fair agreement with the simulated results in Fig. 3, where the ratio at 1000 eV is about 2.4 between swift acceleration mode and standard mode.

The intensity dependence on pass energy for the swift mode acceleration (Fig. 5a) and the ratio between the swift acceleration mode and standard mode (Fig. 5b) are investigated in vacuum using a 0.8 mm slit width. An increasing trend in both peak intensities and the enhancement ratio are found (Fig. 5). Hence, although its performance is superior in all investigated conditions, the swift-acceleration lens table appears to be most powerful under typical high-transmission conditions of large slits and high pass energies.

3.3. High-pressure operation

Pressure dependencies on the intensity of the three peaks (Cu $2p_{3/2}$, Ag $3d_{5/2}$, Au $4f_{7/2}$) in different regimes of the available kinetic electron energy range were recorded with the 1.5 mm slit and a pass energy of 200 eV in both swift-acceleration and standard operation mode. From curve fits of the measured intensity $I(p) = I(0)e^{-kp}$ the exponentially decaying pressure relations, the intensities in vacuum $I(0)$, and the pressure decay constants, k, are determined from Fig. 6a (k_{swift} for swift acceleration mode and $k_{standard}$ for standard mode operation). The resulting data is presented in Table 1 along with calculated intensity enhancement ratios $I(0)_{swift}/I(0)_{standard}$ and decay constant differences $k_{swift} - k_{standard}$.

As demonstrated in Fig. 4 it has already been shown that the Ag $3d_{5/2}$ vacuum peak intensities $I(0)$ are enhanced in the swift-acceleration mode. In Table 1 it is seen that also the Cu $2p_{3/2}$ and Au $4f_{7/2}$ $I(0)$ values are larger, and that the enhancement ratio is about the same for all three peaks in the measured kinetic energy interval of 550 eV–1399 eV. The effect from using the swift-acceleration lens table on the vacuum intensities is apparently significant and of similar strength for different kinetic energies.

The pressure decay constants $k_{standard}$ and k_{swift} decrease with energy, i.e., the signal attenuation is less pronounced at higher kinetic energies, which is in accordance with total electron–N_2 collision cross-sections σ_{lit} in the literature (see Table 2 and [15,16]). Furthermore the transmission through gas of the electrons is significantly higher in the swift-acceleration mode, and, as can be deduced from the $k_{swift} - k_{standard}$ difference values, this effect is strongest for the peak with the lowest kinetic electron energy (Cu $2p_{3/2}$). Taking into account the higher vacuum signals, around 10 to almost 20 times stronger intensity is observed for the three metal peaks under study at sample pressures of 6–8 mbar (see Fig. 6b). These results clearly demonstrate that the swift-acceleration mode is a valuable and time-saving tool in HPXPS.

To analyze the pressure dependence in greater detail it is helpful to decompose the pressure decay constant k into three contributions: (i) $k_{X\text{-}ray}$, the attenuation of the X-ray beam from the X-ray window to the sample; (ii) $k_{outside}$, electron–gas (e–N_2) collisions between the sample and the front cone aperture, where the gas pressure is approximately equal to the pressure in the rest of the analysis chamber; and (iii) k_{inside}, e–N_2 collisions downstream the front cone aperture inside the analyzer front where the gas density

is much lower and ever-diminishing. The X-ray contribution $k_{X\text{-ray}}$ is comparatively small and has been determined as 0.012 $mbar^{-1}$ using a photodiode [6].

By subtracting $k_{X\text{-ray}}$ from k, and assuming that all collisions take place in the 0.8 mm long volume outside the front cone, approximate experimental cross-sections $\sigma_{standard}$ and σ_{swift} are calculated (Table 2). Due to this "outside approximation" the obtained $\sigma_{standard}$ values are larger than the corresponding σ_{lit} values, which indicates that a substantial amount of the collisions occur inside the analyzer (see $\sigma_{standard}/\sigma_{lit}$ section of Table 2). On the contrary the σ_{swift} values are almost equal to the literature data. Our interpretation is that the pressure decay stems almost exclusively from collision events outside the analyzer front in the swift-analyzer mode. This can be understood from the drastic fall in the e–N_2 cross-section from the kinetic energies of the studied Cu, Au, and Ag photoelectrons (550 eV, 1115 eV, and 1399 eV, respectively) to the 4500 eV higher kinetic energies after the swift acceleration in the gap between the front cone aperture and the second cone. As an example the cross-section drops from 4×10^{-16} cm^2 at 500 eV to 0.5×10^{-16} cm^2 at 5000 eV [15,16].

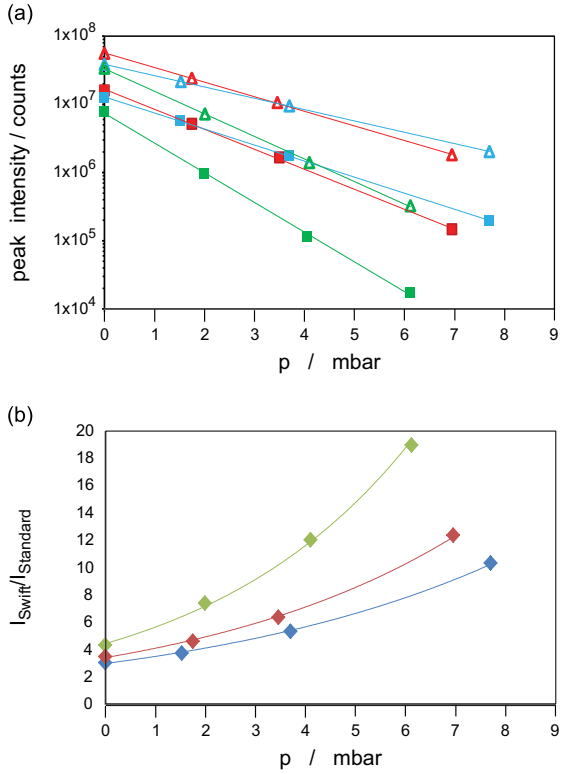

Fig. 6. Pressure dependencies of intensities for Cu $2p_{3/2}$ (green), Ag $3d_{5/2}$ (red), and Au $4f_{7/2}$ (blue) peaks using a pass energy of 200 eV and a slit width of 1.5 mm. (a) Data from the standard and the swift-acceleration lens tables are represented by filled squares and open triangles, respectively. Note that the y-axis has a logarithmic scale. (b) Intensity enhancement for Cu (green diamonds), Ag (red diamonds) and Au (blue diamonds) of the swift acceleration mode compared to the standard table ($I_{swift}/I_{standard}$). (For interpretation of the references to color in this figure legend, the reader is referred to the web version of this article.)

A thorough evaluation of the behavior of the lens tables with N_2 as the sample gas is performed. We expect a similar behavior with most other gases as drastically decreasing electron–molecule collision cross-sections is a quite general characteristic in the 0.5–5 keV regime [15,16]. As an example of this the ability to dramatically enhance the spectrum acquisition time for a Ag 3d core level measured under water vapor (~8 mbar) is shown in Fig. 7. The swift-acceleration measured peaks are about 10 times more intense than the peaks in the standard recording, which agree with the enhancement factor measured for N_2 and Ag. Noteworthy is that there are no signs of discharging in the analyzer front even at these high water pressure levels, in spite of the high field strengths in the swift-acceleration mode.

As discussed in [6], the maximum sample pressure is set both by the front aperture size, the pumping capability of the differentially pumped analyzer front section, and the electron transmission function through the analyzer. Due to the improved transmission the swift-acceleration mode is anticipated to push the optimum range for the 0.8 mm cone upwards in pressure. Reduced electron losses from the swift acceleration are also anticipated with the smaller cone aperture sizes (0.3 mm and 0.5 mm). A consequence of the extended pressure regime is that larger front cone apertures can be used in HPXPS, giving improved electron collection and facilitating the use of large X-ray sample spots. The ability to use a larger collection area is that a lower flux can be used which is beneficial for radiation sensitive samples.

3.4. Outlook: high pressure surface science

To further show the capabilities and test the swift acceleration mode of the HPXPS instrument a more technologically relevant sample, an organic monolayer on a semiconductor surface, was measured and compared to similar measurements recorded at a synchrotron UHV based photoelectron spectroscopy setup. Such systems are interesting in energy applications such as catalysis [3,17] and solar cells [18,19]. Since electrochemistry usually involves a solid–liquid interface, HPXPS is a very suitable tool to gain new insights in these complex systems. Here a mesoscopic TiO_2 surface sensitized with a Ru-based dye molecule (Z907) [19] was measured under a 2 mbar H_2O atmosphere. Similar measurements have been performed before in vacuum using synchrotron-based measurements [11]. As seen in Fig. 8 the HOMO peak of the dye molecule is clearly visible both in vacuum and water atmosphere around 1.5 eV binding energy. The HOMO peak mainly consists of Ru 4d [12]. The large feature between 2 and 8 eV originates from TiO_2 and the structure around 10 eV, which is only visible in the water spectrum [20], is the valence band of water in gas phase. A more detailed description of the Z907 dye and the effect from water, measured

Table 2
Total e–N_2 cross-sections from the literature (σ_{lit}) and the present experimental data ($\sigma_{standard}$, σ_{swift}).

Peak	Kinetic energy (eV)	σ_{lit} (10^{-16} cm^2)	$\sigma_{standard}$ (10^{-16} cm^2)	σ_{swift} (10^{-16} cm^2)	$\sigma_{standard}/\sigma_{lit}$
Cu $2p_{3/2}$	550	3.4	4.5	3.3	1.3
Ag $3d_{5/2}$	1115	2.0	2.9	1.9	1.5
Au $4f_{7/2}$	1399	1.6	2.2	1.3	1.4

Table 1
Fitted parameter values from the pressure curves in Fig. 6.

Peak	Kinetic energy (eV)	$I(0)_{standard}$	$I(0)_{swift}$	$k_{standard}$ ($mbar^{-1}$)	k_{swift} ($mbar^{-1}$)	$I(0)_{swift}/I(0)_{standard}$	$k_{standard} - k_{swift}$ ($mbar^{-1}$)
Cu $2p_{3/2}$	550	7510^6	3010^7	1.00	0.76	4	0.24
Ag $3d_{5/2}$	1115	2110^7	6010^7	0.68	0.49	3	0.19
Au $4f_{7/2}$	1399	1310^7	4010^7	0.54	0.38	4	0.16

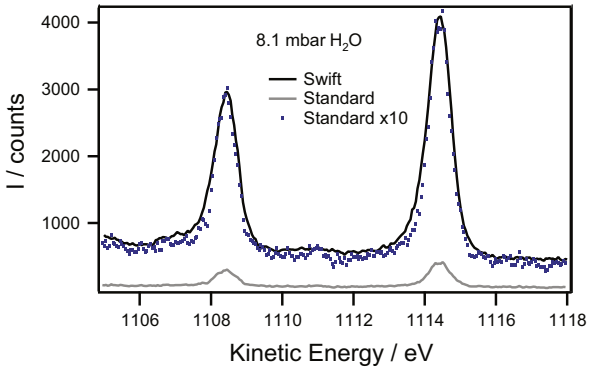

Fig. 7. Ag 3d peak profiles with 8.1 mbar water vapor obtained with the standard (gray line) and swift-acceleration (black line) lens tables at a pass energy of 200 eV and a slit width of 1.5 mm. In order to illustrate the enhancement of the swift acceleration mode a $\times 10$ enhancement of the standard mode spectrum is included in the graph (blue dots). (For interpretation of the references to color in this figure legend, the reader is referred to the web version of this article.)

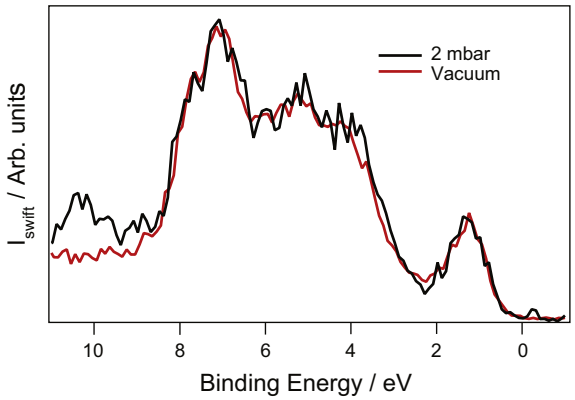

Fig. 8. The valence band of nanostructured TiO_2 sensitized with the Ru based dye molecule Z907. The peak at 1.5 eV is the HOMO of the dye and the large feature between 2 and 8 eV stems from TiO_2. A water valence band feature is seen around 10 eV in the spectrum subjected to water vapor.

using HPXPS, will be detailed in a future publication. Remarkably the acquisition time at 2 mbar H_2O pressure was just less than 1 h for a 12 eV wide scan, as displayed in Fig. 8. For the spectra a step size of 0.1 eV, dwell time of 0.2 s, pass energy of 200 eV, and an entrance slit size of 0.8 mm was used. The corresponding spectrum measured at a synchrotron (with lower photon energy) was acquired in vacuum in ~20 min [12].

4. Conclusions

By comparing the dependence of peak shapes and photoelectron intensity on a broad range of experimental parameters it is found that the new HPXPS transmission mode with swift-acceleration of electrons emitted within the analyzer front is superior to traditional field-free or low-field "standard" operation for nearly all meaningful situations, and in particular under typical high-transmission conditions of wide-open slits and high pass energies. This is also true regarding the resolution, as smaller slits (and higher resolution) can be applied with the swift-acceleration mode to give comparable spectral acquisition times. It is emphasized though that the swift-acceleration mode is tailored for systems with an Al Kα X-ray source or other excitation sources with photon energies of at most a few KeV. Using higher photon excitation energies, at synchrotron facilities, would not give the same pronounced effects at high pressures as the electron scattering cross-sections are much lower at high kinetic energies. Furthermore the simulation results (Fig. 3) indicate that the swift-acceleration mode will not be efficient in vacuum measurements for higher kinetic energies.

The new swift-acceleration transmission mode pushes the limits for what can be measured with reasonable spectral acquisition times using home laboratory HPXPS systems. Probing photoelectrons from energetically deeper electronic states, with low kinetic energies and consequently short mean-free-paths in the gas, now becomes feasible. The achievable pressure regime for the used 0.8 mm front cone is anticipated to extend upwards by 2–4 mbar, which is deduced from Fig. 6 by comparing equal intensity levels of the swift-acceleration and standard operation pressure curves. A consequence of the extended pressure regime is that larger front cone apertures can be used in HPXPS, giving improved electron collection and facilitating the use of large X-ray sample spots. For example, this feature is desirable for radiation-sensitive samples, which is demonstrated by recording valence band spectra of the molecularly modified oxide surface used in for example dyes-sensitized solar cells. Here the swift acceleration operation mode speeds up the recording time significantly for beam damage prone samples. Furthermore the pumping requirements in the analyzer front become less critical, which therefore has the potential benefit of bringing down the costs, and maintenance requirements for HPXPS home lab systems.

Acknowledgment

This work was supported by the Swedish Governmental Agency for Innovation Systems (VINNOVA). S.K.E, M.H, H.S, H.R. gratefully acknowledge StandUp for Energy, Swedish Energy Agency, the Swedish Research Council (Grant nos. 2012-4681, and 2012-4721) for financial support. D.J.P. acknowledges support from the Royal Society (UF100105). J.M.K. acknowledges support from the EPSRC for a Doctoral Prize Studentship. D.J.P and I.J.V.G acknowledge support from the EPSRC (EP/K004913/1 and EP/J021199/1).

References

[1] D.E. Starr, et al., Chemical Society Reviews 42 (13) (2013) 5833.
[2] F. Mangolini, et al., Review of Scientific Instruments 83 (2012) 9.
[3] S. Kaya, et al., Catalysis Today 205 (2013) 101.
[4] H. Bluhm, Journal of Electron Spectroscopy and Related Phenomena 177 (2-3) (2010) 71.
[5] D.F. Ogletree, et al., Nuclear Instruments and Methods in Physics Research Section A: Accelerators Spectrometers Detectors and Associated Equipment 601 (1-2) (2009) 151.
[6] S.K.e.a., Eriksson, HiPP. Review of Scientific Instruments 85 (2014) 075119. http://dx.doi.org/10.1063/1.4890665.
[7] K. Roy, C.P. Vinod, C.S. Gopinath, The Journal of Physical Chemistry C 117 (9) (2013) 4717.
[8] F. Tao, Chemical Communications 48 (32) (2012) 3812.
[9] N. Martensson, et al., Journal of Electron Spectroscopy and Related Phenomena 70 (2) (1994) 117.
[10] B. Wannberg, Nuclear Instruments and Methods in Physics Research Section A: Accelerators, Spectrometers, Detectors and Associated Equipment 601 (1–2) (2009) 182.
[11] M. Hahlin, et al., Journal of Physical Chemistry C 115 (24) (2011) 11996.
[12] E.M.J. Johansson, et al., Journal of Chemical Physics 126 (2007) 24.
[13] D.F. Ogletree, et al., Review of Scientific Instruments 73 (11) (2002) 3872.
[14] G. Drera, et al., Transmission function calibration of an angular resolved analyzer for X-ray photoemission spectroscopy: theory vs experiment. Journal of Electron Spectroscopy and Related Phenomena, Journal of Electron Spectroscopy and Related Phenomena 195 (2014) 109–116.
[15] G. Garcia, A. Perez, J. Campos, Physical Review A 38 (2) (1988) 654.
[16] Y. Itikawa, Journal of Physical and Chemical Reference Data 35 (1) (2006) 31.
[17] A. Hagfeldt, et al., Chemical Reviews 110 (11) (2010) 6595.
[18] B. Oregan, M. Gratzel, Nature 353 (6346) (1991) 737.
[19] S.M. Zakeeruddin, et al., Langmuir 18 (3) (2002) 952.
[20] K. Kimura, Handbook of Hel Photoelectron Spectra Of Fundamental Organic Molecules, Japan scientific societies press, Tokyo Halsted press, New York (1981) 268.